Copyright © 1990, by the author(s).
All rights reserved.

Permission to make digital or hard copies of all or part of this work for personal or classroom use is granted without fee provided that copies are not made or distributed for profit or commercial advantage and that copies bear this notice and the full citation on the first page. To copy otherwise, to republish, to post on servers or to redistribute to lists, requires prior specific permission.

CHARACTERIZATION OF THE PROCESSING PLASMA IN AN ENGINEERING PROTOTYPE REACTOR FOR PLASMA IMMERSION ION IMPLANTATION

by

R. A. Stewart, X. Y. Qian, D. A. Carl, B. Lake, Jr.,
J. Benasso, R. Lynch, C. A. Pico, M. A. Lieberman,
and N. W. Cheung

Memorandum No. UCB/ERL M90/100

12 November 1990

CHARACTERIZATION OF THE PROCESSING PLASMA IN AN ENGINEERING PROTOTYPE REACTOR FOR PLASMA IMMERSION ION IMPLANTATION

by

R. A. Stewart, X. Y. Qian, D. A. Carl, B. Lake, Jr., J. Benasso, R. Lynch, C. A. Pico, M. A. Lieberman, and N. W. Cheung

Memorandum No. UCB/ERL M90/100

12 November 1990

ELECTRONICS RESEARCH LABORATORY

College of Engineering
University of California, Berkeley
94720

CHARACTERIZATION OF THE PROCESSING PLASMA IN AN ENGINEERING PROTOTYPE REACTOR FOR PLASMA IMMERSION ION IMPLANTATION

by

R. A. Stewart, X. Y. Qian, D. A. Carl, B. Lake, Jr., J. Benasso,
R. Lynch, C. A. Pico, M. A. Lieberman, and N. W. Cheung

Memorandum No. UCB/ERL M90/100

12 November 1990

ELECTRONICS RESEARCH LABORATORY

College of Engineering
University of California, Berkeley
94720

ABSTRACT

An engineering prototype reactor has been developed to study plasma immersion ion implantation as an integrated circuit fabrication technique. The reactor consists of an electron cyclotron resonance source, a processing chamber with wafer bias supply, gas handling and plasma diagnostic tools. Wafers up to 250 mm in diameter can be processed, to demonstrate single-wafer processing of large diameter wafers. The experimental apparatus is described, and the results of Langmuir probe measurements characterizing an argon plasma in the process chamber is presented.

1. INTRODUCTION

Ion implantation is an important technique in integrated circuit fabrication. Due to the continuing trend toward smaller, faster and more densely packed circuitry, conventional ion implantation technology faces several challenges. Two major challenges are throughput, which is limited by the available ion current, and the production of very low energy ion beams for shallow implants. Other important concerns include charging, channeling, shadowing and damage.

An alternative to conventional ion implantation that may eliminate several of the above problems is *plasma immersion ion implantation* (PIII). This technique was orininally demonstrated by Conrad [1] and Tendys [2] as a method to improve wear and hardness of materials such as metals, plastics and ceramics for industrial applications. Recently [3-5], PIII has been successfully applied to semiconductor device fabrication for a number of VLSI applications including sub-100 nm p+/n junction formation, conformal implantation for trench doping and palladium seeding for electroless Cu plating.

Several features of PIII make it an attractive alternative to conventional ion implantation. With the high current capability of PIII, the throughput of present integrated circuit steps can be substantially increased. Also, the intermediate step of the ion source and all of its support equipment is completely eliminated. Ions that are created in an electron cyclotron resonance (ECR) plasma source, diffuse into a process chamber where they are extracted directly from the process plasma in which the wafer holder is located. The substrate holder is biased to a high negative voltage and the ions are accelerated to the wafer through a high voltage plasma sheath. Since the ion energy is controlled by the applied voltage, very low energy implants ($\leq$ 1 keV) are possible. In addition, since PIII operates with an ECR plasma discharge, a range of pressures from 0.1-100 mTorr may be used. Thus, the angular distribution of the implanted ions can be adjusted simply by varying the gas pressure. This feature is very attractive for conformal doping of nonplanar surface topographies such as high-aspect-ratio trenches.

PIII can also operate in a triode mode by introducing a sputtering target near to or within the ECR source chamber. The sputtering rate can be controlled by applying a suitable bias to the target. This technique provides the capacity of implanting any solid material into the substrate as long as the material has reasonable sputtering and ionization rates. In addition, dual ion implantations of both the source and sputtered atomic species can be achieved by varying the target and wafer holder biases.

In this paper, a recently constructed engineering prototype reactor (EPR) is described. The new reactor, is considerably scaled up in size from the reactor reported by Qian [6]. This reactor was designed to investigate issues such as implant uniformity over large areas, reproducibility, reactor materials compatibility with IC process requirements, cleanliness of the reactor environment, and other applications of PIII related to integrated circuits processing. In addition, the large process chamber will

facilitate basic studies of the process plasma physics through the use of several diagnostic techniques.

Extensive characterization of argon plasmas in the EPR with Langmuir probe measurements has been completed. Results are presented for ion density and electron temperature over a wide range of variation of the control parameters, e.g., microwave power, gas pressure and magnetic field configuration.

2. REACTOR DESCRIPTION

The new EPR is shown in Fig. 1. The system is powered by a 1500 W ASTEX ECR 2.45 GHz microwave source. Power is coupled into the 14 cm I.D., 40 cm long source chamber through a quartz window using a TE_{10} rectangular to TM_{01} circular mode converter which reduces azimuthal plasma nonuniformities and provides increased radial uniformity over conventional coupling schemes. The plasma is created mainly in the source chamber and then expands into a 43.2 cm I.D., 81 cm long process chamber where the implantation takes place. The vacuum system consists of a 1000 liter/s Leybold-Heraeus turbomolecular pump for corrosive gas handling backed by a 46 ft^3/min Leybold-Heraeus mechanical pump. The system pressure is feedback controlled over the range of 0.1-100 mTorr. Control circuitry has been designed in conjunction with a thermocouple controller to automate the vacuum system pumping/venting sequence as well as to provide numerous interlocks for protection against vacuum or power failure. A gas manifold allows for easy switching between different process gases, as well as regular venting of gas lines through the mechanical pump following the use of corrosive gases. Mirror magnetic fields are generated by two 120 turn water cooled coils 22.9 cm I.D., 50.8 cm O.D. and 15 cm thick powered by a regulated d.c. supply. The coils are mounted on rollers so that the magnetic field configuration can easily be

adjusted. For the results reported here, the spacing between coil midplanes was 31 cm and the midplane at the rear coil was located 2.2 cm in front of the quartz vacuum window.

Both the source and process chambers were made from aluminum for *materials* compatibility with the usual IC processes. The system will also accept various liners (quartz, graphite, silicon) if increased process purity is required. The source and process chambers have many ports to allow both for visual inspection as well as access to the plasma by diagnostics tools such as Langmuir probes and optical emission spectroscopy.

A 25 cm aluminum wafer holder is used to suspend wafers up to 250 mm in diameter in the plasma. The wafer holder's axial position in the process chamber can be continuously varied between ports 3 and 5, indicated in Fig. 1a. In addition, the holder can be rotated about its vertical axis to any arbitrary angular orientation. The holder is loaded into and out of the top of the process chamber by means of a motor driven crane. The holder's support framework provides thermal isolation from outside the chamber by means of an alumina rod, and the wafer holder can be cryogenically cooled. Electrical feedthrough from a pulse generator to the holder in order to bias the substrate is acheived using wafer biasing is achieved using the aluminum liquid nitrogen lines.

3. PLASMA CHARACTERIZATION

Initial characterization of the EPR has been carried out. Base pressures of 5×10^{-7} Torr have been obtained to date. The magnetic field profile has been measured with Hall probes. Axial profiles of $B(z)$ are plotted in Fig. 2 for 3 different magnet currents I_m with a fixed spacing of 31 cm between the magnets. Note that for

$I_m \gtrsim 220$ A, this mirror configuration results in up to three distinct ECR zones. Studies of argon plasmas have been carried out to evaluate reproducibility and tunability with respect to input microwave power. Here, we define a reproducible plasma as one that for a given set of control parameters (i.e., gas pressure, magnet current, input microwave power and tuning stub settings), consistently results in zero reflected power. That is, each time the plasma is struck, it should be well tuned. For the fields indicated in Fig. 2, and over a wide range of gas pressure and input power, argon plasmas were found to be most easily tunable and reproducible with a magnet current $I_m = 240$ A. Argon plasmas have been sustained for pressures $\geq$ 0.1 mTorr, with tunability generally improving as pressure is increased. Similarly, tunability generally increases as the input power is increased.

Extensive measurements of the plasma in the process chamber have been made with Langmuir probes. Details of the probe construction and measurement circuitry are shown in Figs. 3 and 4, respectively. Very thin tungsten wire 0.076 mm in diameter and ranging from 7-10 mm in length was used to collect the current. Measurements consist either of obtaining complete I-V characteristics at a given probe position or just measuring a single (V, I) data point at a bias voltage of -35 V in the ion saturation portion of the I-V characteristic. The former method allows one to extract plasma density and electron temperature, while the latter yields only plasma density and was used for uniformity studies. Using Laframboise's analysis [7] for the orbital motion limited case, the (ion) density n_i was related to the probe current measured by the relation:

$$n_i = \frac{I_{pr}}{e r_{pr} l_{pr} \sqrt{\frac{-8 e V_{pr}}{m_i}}} \tag{1}$$

where e is the electron charge, m_i is the ion mass, I_{pr} is the probe current, V_{pr} is the probe voltage, and r_{pr} and l_{pr} are the probe's radius and length, respectively. Use of (1) is justified (see Fig. 40 of [7]) since we calculate $r_{pr}/\lambda_D \lesssim 1$, where λ_D is the electron Debye length. Electron temperature was calculated from the slope of $\ln(I_e)$ vs. V_{pr} *in* the electron retardation portion of the *I-V* curve. The floating potential V_f was also measured by using a probe to directly record the voltage in the plasma at a given position with a voltmeter. The plasma potential V_p was then calculated using the relation [8]:

$$V_p = V_f + (kT_e/2e)\ln(m_i/2.3m_e) \tag{2}$$

where k is Boltzmann's constant and m_e is the electron mass.

Most probe measurements were taken with the wafer holder located just behind port 4 (see Fig. 1a). The presence of the holder has not been found to affect the plasma generation process; we have found that measurements taken at port 4 with the holder present (probe $\approx$ 1 cm in front of holder), indicate a reduction in plasma density of approximately 50% from the density measured in the absence of the holder. Also, the average plasma density $\approx$ 1 cm behind the holder is roughly one-tenth of the density measured in front of the holder, indicating that for PIII, the rear surface of the wafer holder has a small effect on the overall ion collection area.

Results of several measurements taken at port 4, centerline are shown in Figs. 5-7, 9. In Fig. 5, microwave power scans of plasma (ion and electron) density are shown for pressures, p, ranging from 0.1-5 mTorr. For these data the reflected power was typically less than 1% of the input power. The curves exhibit a roughly linear dependence of density on input power, P. Further increase in pressure above 5 mTorr

leads to a reduced ion density. As indicated in Fig. 6 for $P = 500$ W, the ion density peaks at about $p = 5$ mTorr and then drops off as pressure is increased further. In Fig. 7 the electron temperature is plotted versus pressure for $P = 500$ W. For comparison with the pressure scans in Figs. 6 and 7, similar plots are shown in Fig. 8 for the smaller ECR reactor used by Qian [6]. Qualitatively similar behavior exists between the corresponding plots for each reactor, suggesting that the process plasmas in each reactor are similar. A final plot at port 4, centerline is shown in Fig. 9. Electron temperature, floating potential and plasma potential are all relatively insensitive to input power. A similar plot of these three plasma parameters versus distance along the axis of the process chamber is shown in Fig. 10. Beyond port 1, these quantities exhibit little change with distance from the end of the source chamber. The electron temperature near the wafer holder is seen to be about 2 eV.

The remaining measurement results demonstrate the degree of radial uniformity exhibited by the ion density. Unless otherwise noted, the wafer holder was located just behind port 4. The center of the wafer holder was located on the axis of the chamber and the plasma was probed every 2.54 cm along a tranverse axis (accessed from one of the ports). In Fig. 11, the radial variation $n_i(r)$ of ion density is plotted for ports 1-4 with $p = 1$ mTorr and $P = 500$ W. The double-humped, slightly asymmetric radial profile of the plasma emerging from the source chamber is clearly evident and, despite radial diffusion of the downstream plasma, this initial nonuniformity persists somewhat up to the location of the wafer holder at port 4. Figs. 12 and 13 contain several plots of normalized ion density at port 4, showing how radial uniformity is affected by power and pressure, respectively. For the argon plasma probed, the greatest degree of uniformity ($\sim 4\%$ variation from maximum to minimum over a diameter of 16 cm) was obtained for $p = 1$ mTorr and $P = 300$ W. To investigate the influence of magnet current on radial uniformity, the plots of Figs. 12 and 13 (taken with $I_m = 240$ A) were

repeated with $I_m = 220$ A and are shown in Figs. 14 and 16. The uniformity is seen to be significantly better with $I_m = 240$ A. As a final radial plot, Fig 16 shows plots of floating potential V_f versus radial position for ports 1-3. Notable is the large gradient dV_f/dr in the port 1 plot. The radial location of this large gradient corresponds to the radial position where the ion density falls rapidly in Fig. 11. These results suggest that as the plasma streams out of the source chamber, the magnetized electrons are forced to follow the slowly diverging magnetic field lines, while the ions diffuse radially outward.

4. CONCLUSIONS

A new engineering prototype reactor designed for PIII applications has been described. The reactor consists of an ECR plasma source and a large 43.2 cm I.D. process chamber for implanting large area wafers.

Results of Langmuir probe measurements in an argon plasma have been presented. The plasma reproducibility and dependence of ion density, electron temperature, plasma potential and floating potential on external control parameters including power, pressure, and magnetic field configuration have been investigated. For the coil positioning used, a current of 240 A results in the most stable, tunable plasma. A discharge is sustainable for pressures exceeding 0.1 mTorr, and generally, tunabilility increases with increasing pressure and power. The variation of ion density with pressure and power is qualititively consistent with the extensive literature already published on ECR reactor plasmas.

Radial plots of ion density reveal that the downstream process plasma radial profile is due primarily to residual nonuniformities from the asymmetric density profile streaming out of the source chamber. Further studies will be made to help improve the radial uniformity. In particular, investigation of other magnet spacings and positionings

will be carried out to seek conditions that lead to a more uniform ECR plasma. Concurrently, theoretical modeling of the ECR physics will be carried out to develop a basis for understanding and predicting plasma mode shapes. Another method for improving uniformity in the process chamber consists of placing permanent magnets on the surface of the process chamber to create a confining "magnetic bucket". This latter technique is expected to improve uniformity more or less independently of the input power and pressure.

ACKNOWLEDGEMENTS

This work is supported by Applied Materials, Inc. and a grant from the California State MICRO program.

REFERENCES

[1] J. R. Conrad, J. L. Radtke, R. A. Dodd, F. J. Worzala and N. C. Tran, *J. Appl. Phys.* 62, 4591, (1987).

[2] J. Tendys, I. J. Donnelly, M. J. Kenny and J. T. A. Pollock, *Appl. Phys. Lett.* **53** (22), 2143, (1988).

[3] X. Y. Qian, N. W. Cheung, M. A. Lieberman, M. I. Current, P. K. Chu, W. L. Harrington, C. W. Magee and E. M. Botnick, *Proceedings of the VIII International Conference on Ion Implantation Technology*, July 31-August 3, 1990, University of Surrey, United Kingdom.

[4] X. Y. Qian, N. W. Cheung, M. A. Lieberman, R. Brennan, M. I. Current and N. Jha, ibid.

[5] X. Y. Qian, M. H. Kiang, J. Huang, D. A. Carl, N. W. Cheung, M. A. Lieberman, I. G. Brown, K. M. Yu and M. I. Current, ibid.

[6] X. Y. Qian, D. A. Carl, J. Benasso, N. W. Cheung, M. A. Lieberman, I. G. Brown, J. E. Galvin, R. A. MacGill and M. I. Current, ibid.

[7] J. G. Laframboise, Inst. for Aero. Stud., Univ. of Toronto, Rep. No. 100 (1966), Sect. 14 and Fig. 40.

[8] S. M. Gorbatkin, L. A. Berry, and J. B. Roberto, *J. Vac. Sci. Technol.* A 8, 2893, (1990).

FIGURE CAPTIONS

Fig. 1 (a) Schematic side view of the PIII engineering prototype reactor. (b) Scaled diagram of the reactor showing a side view of the actual physical layout.

Fig. 2 Axial magnetic field profile measured as a function of distance from the ECR chamber's quartz window for $I_m = 200$, 220 and 240 A.

Fig. 3 Details of Langmuir probe construction.

Fig. 4 Biasing circuit used to make probe measurements.

Fig. 5 Ion density as a function of power for $p = 0.1$, 0.5, 1.0 and 5 mTorr. Measured at port 4, centerline with $I_m = 240$ A.

Fig. 6 Ion density as a function of pressure for $P = 500$ W. Measured at port 4, centerline with $I_m = 240$ A.

Fig. 7 Electron temperature as a function of pressure for $P = 500$ W. Measured at port 4, centerline with $I_m = 240$ A.

Fig. 8 (a) Ion density as a function of pressure for $P = 550$ W in a small ECR reactor used by Qian [6]. (b) Electron temperature as a function of pressure for $P = 550$ W in a small ECR reactor used by Qian [6].

Fig. 9 Electron temperature, floating potential and plasma potential as a function of

power for $p=1$ mTorr. Measured at port 4, centerline with $I_m=240$ A.

Fig. 10 Electron temperature, floating potential and plasma potential as a function of distance from the source chamber for $p=1$ mTorr, $P=500$ W. Measured at ports 1-5, centerline with $I_m=240$ A.

Fig. 11 Radial ion density profile for $p=1$ mTorr, $P=500$ W. Measured at ports 1-4 with $I_m=240$ A.

Fig. 12 Radial ion density profile for $p=1$ mTorr, $P=300$, 500 and 800 W. Measured at port 4 with $I_m=240$ A.

Fig. 13 Radial ion density profile for $p=0.25$, 1.0 and 5.0 mTorr, $P=500$ W. Measured at port 4 with $I_m=240$ A.

Fig. 14 Radial ion density profile for $p=1$ mTorr, $P=300$, 500 and 800 W. Measured at port 4 with $I_m=220$ A.

Fig. 15 Radial ion density profile for $p=0.5$, 1.0 and 5.0 mTorr, $P=500$ W. Measured at port 4 with $I_m=220$ A.

Fig. 16 Floating potential radial profile for $p=1$ mTorr, $P=500$ W. Measured at ports 1-3 with $I_m=240$ A.

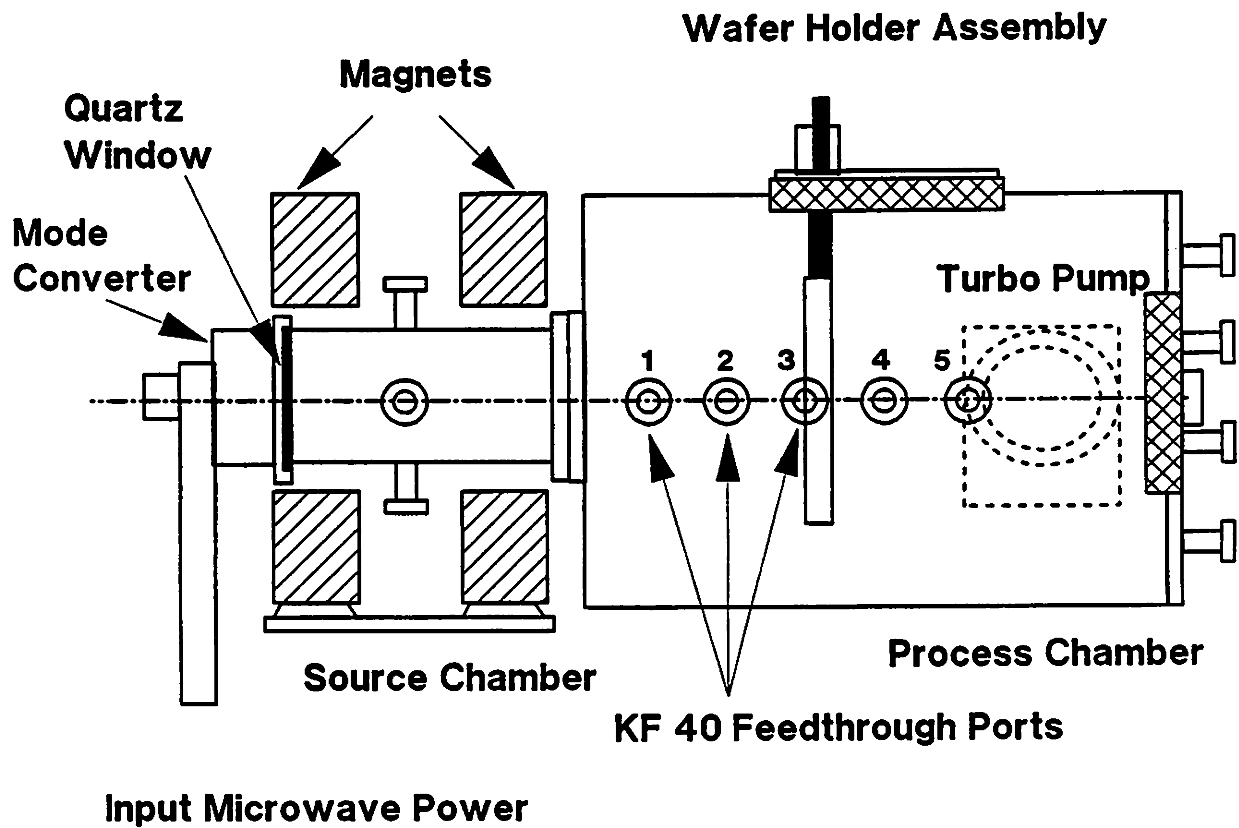

Figure 1(a)

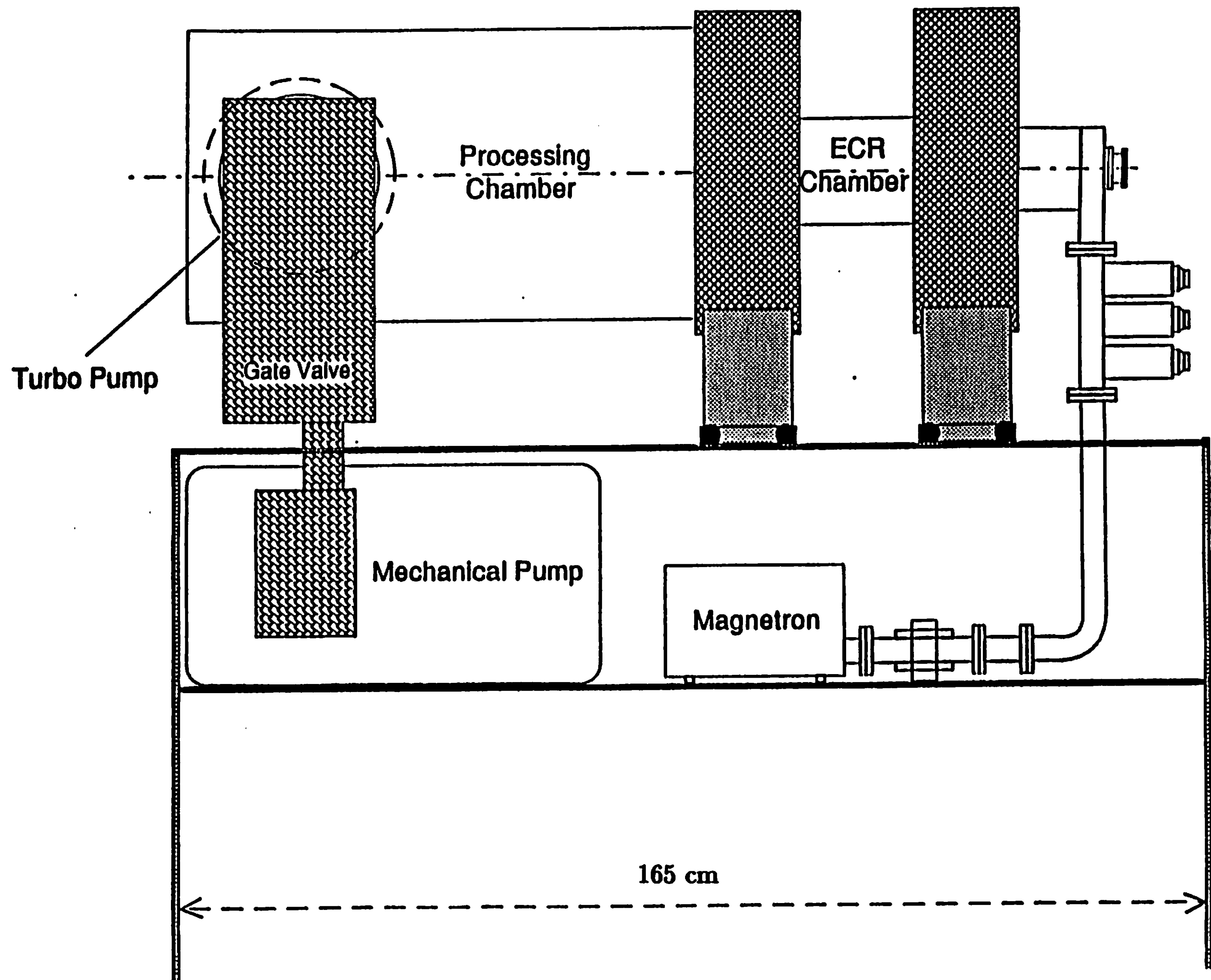

Scale: 1/10 (1 cm ⇒ 10 cm)

Figure 1(b)

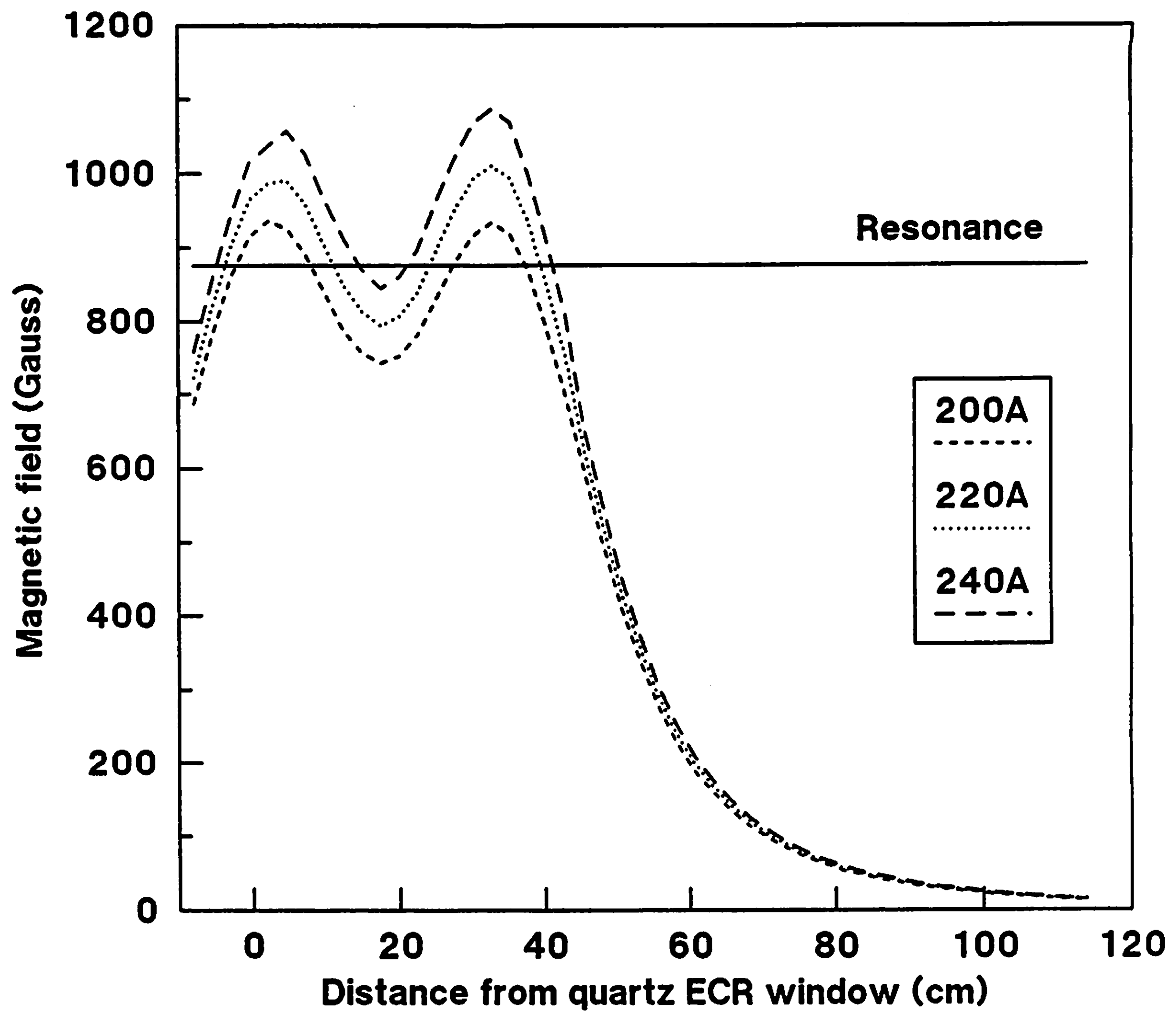

Figure 2

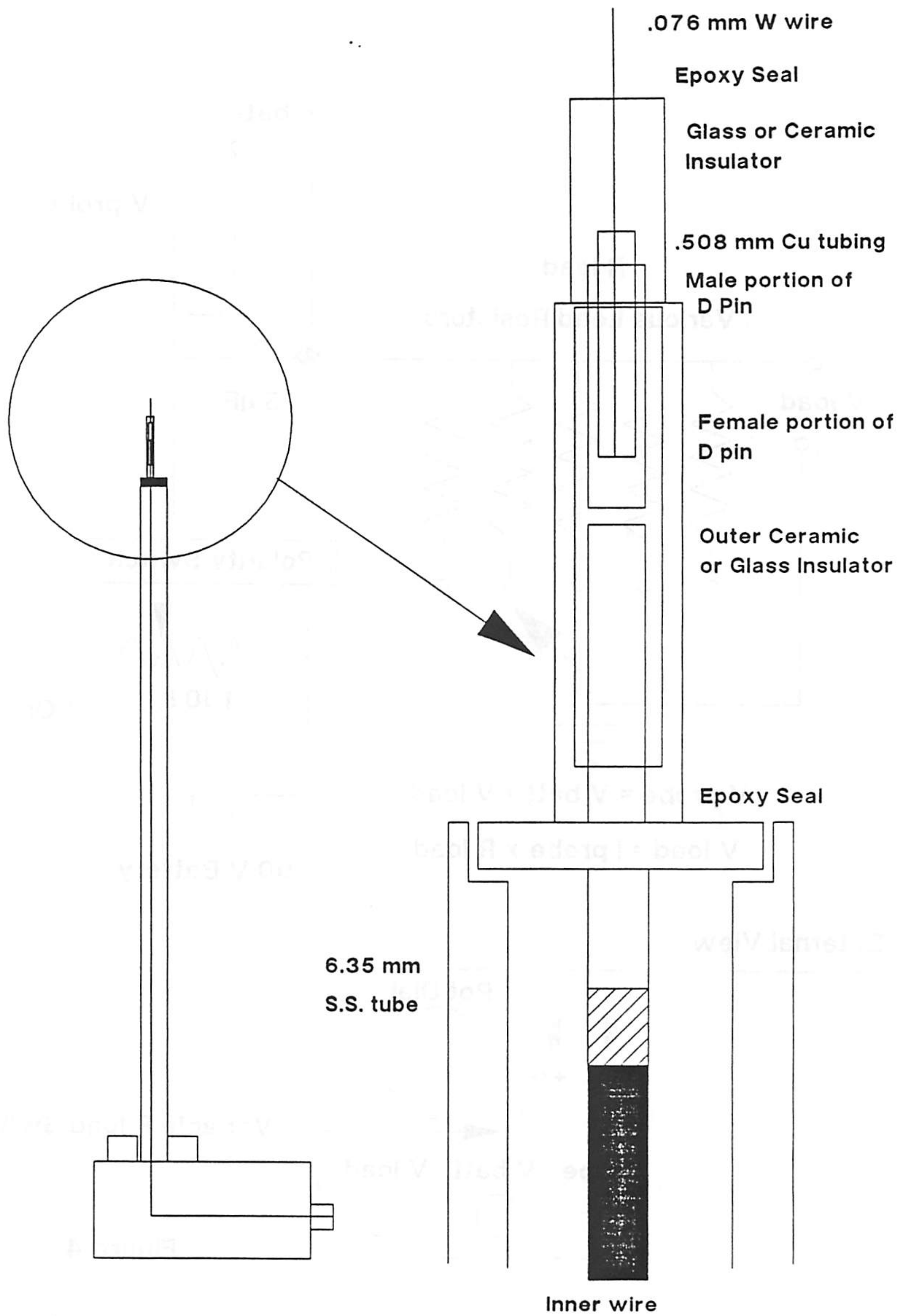

Figure 3

V batt

V probe

R load

Various Load Resistors

V load

5 uF

Polarity Switch

100 K

On/Off

V probe = V batt + V load

V load = I probe x R load

90 V Battery

External View

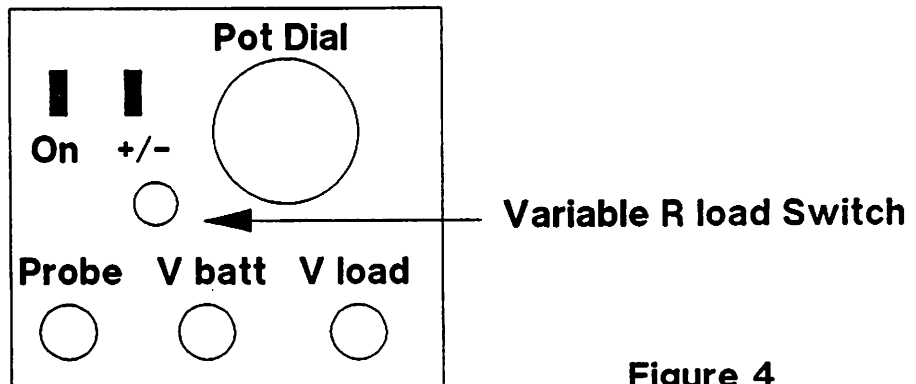

Figure 4

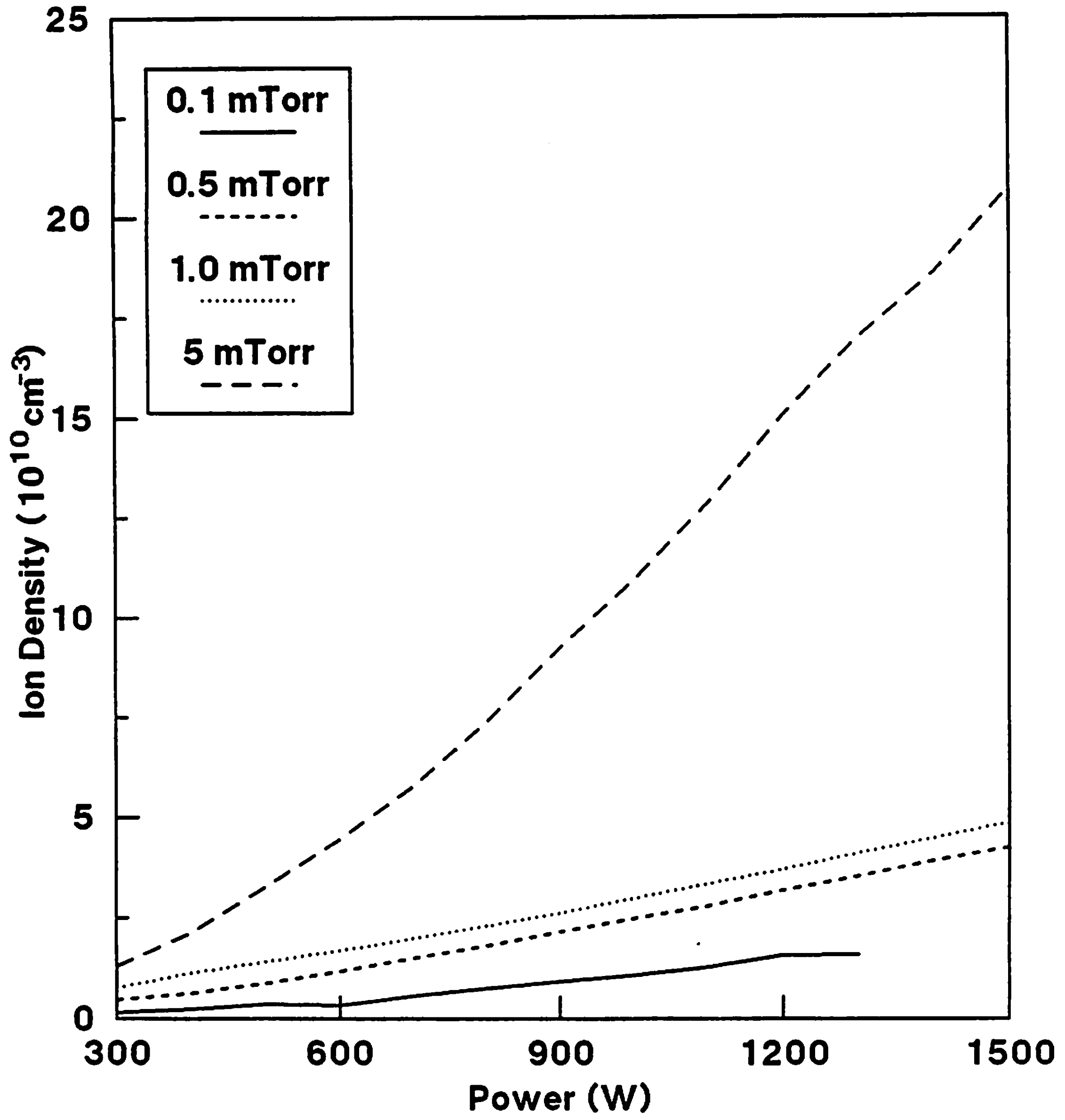

Figure 5

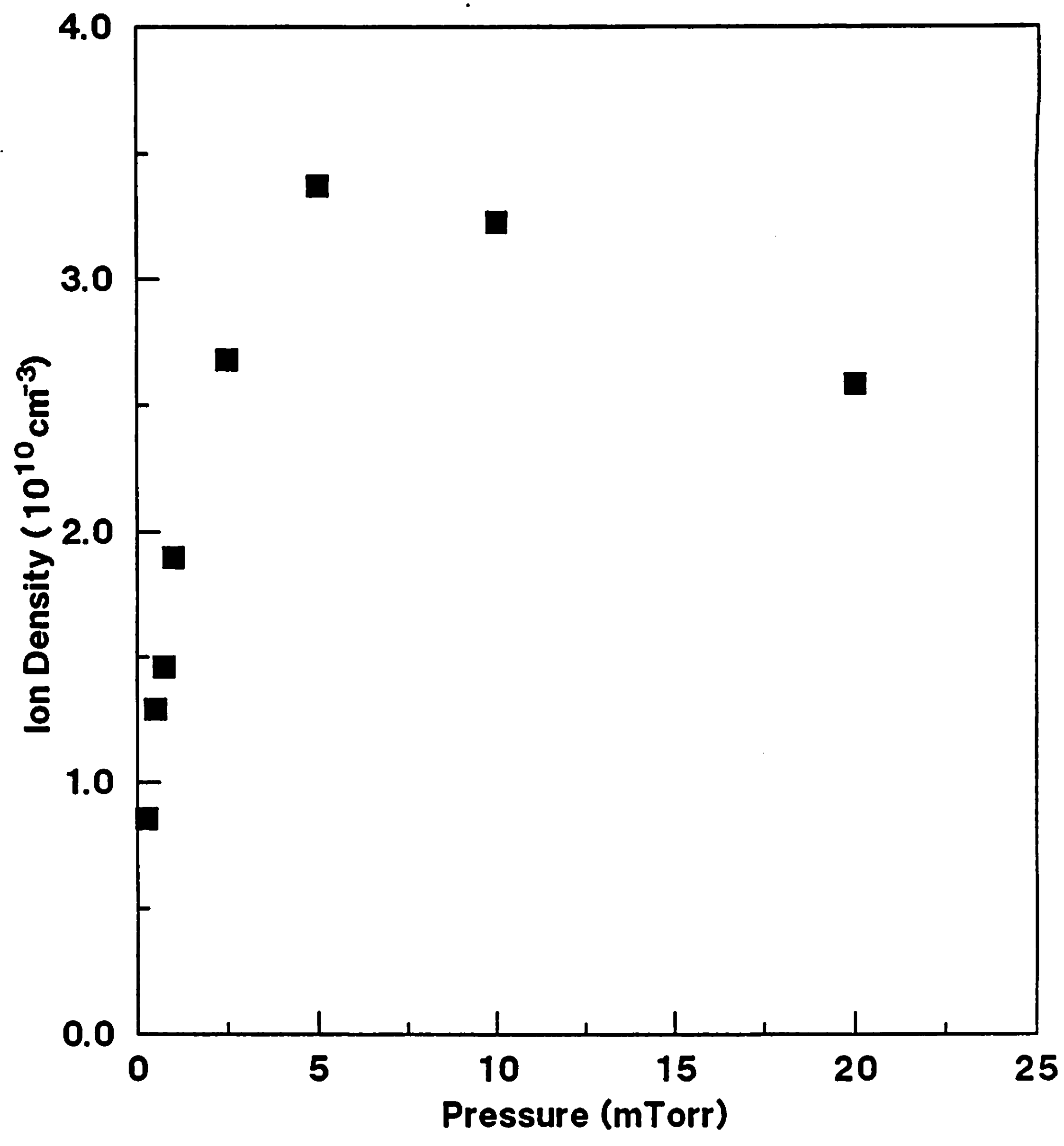

Figure 6

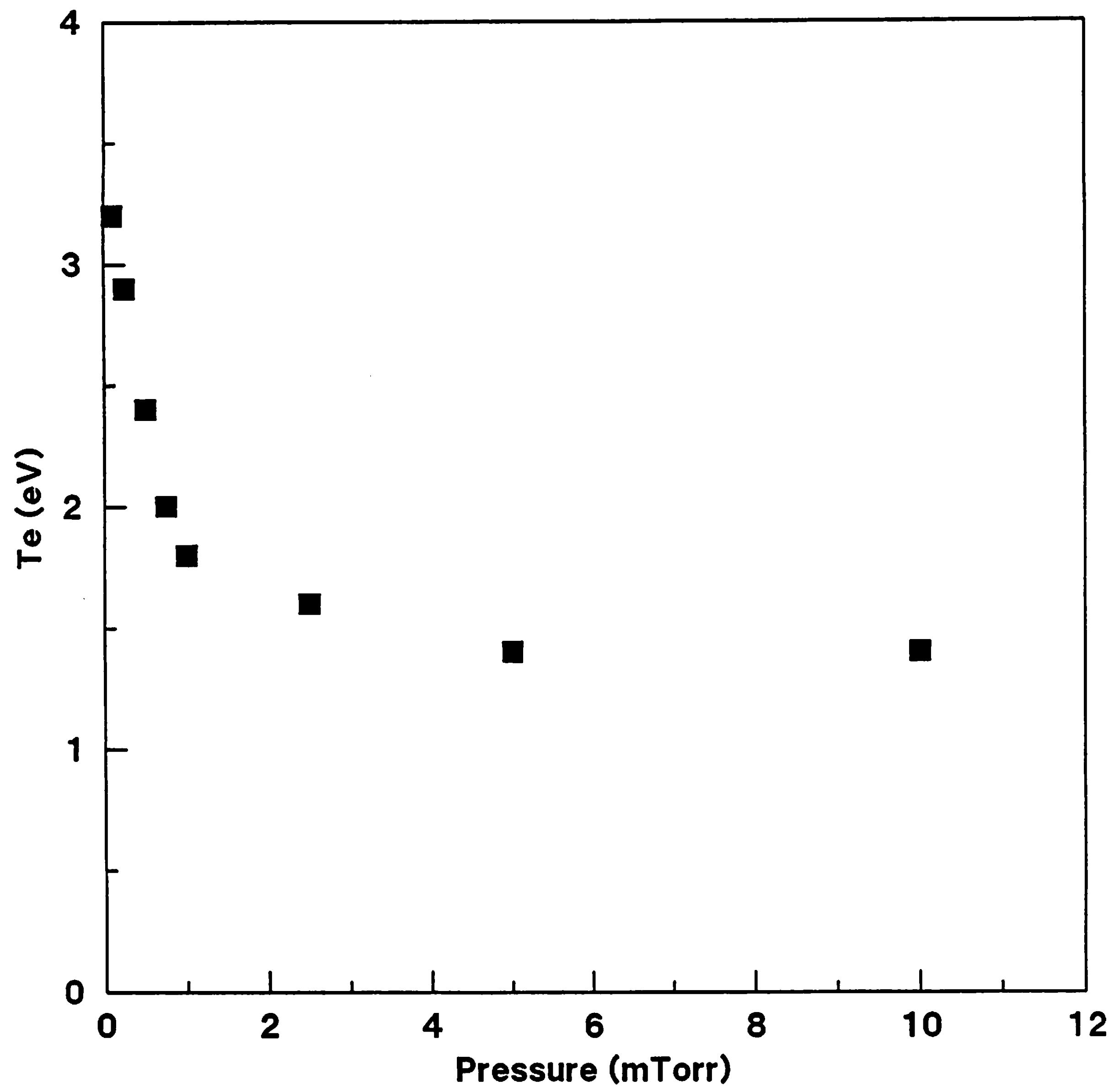

Figure 7

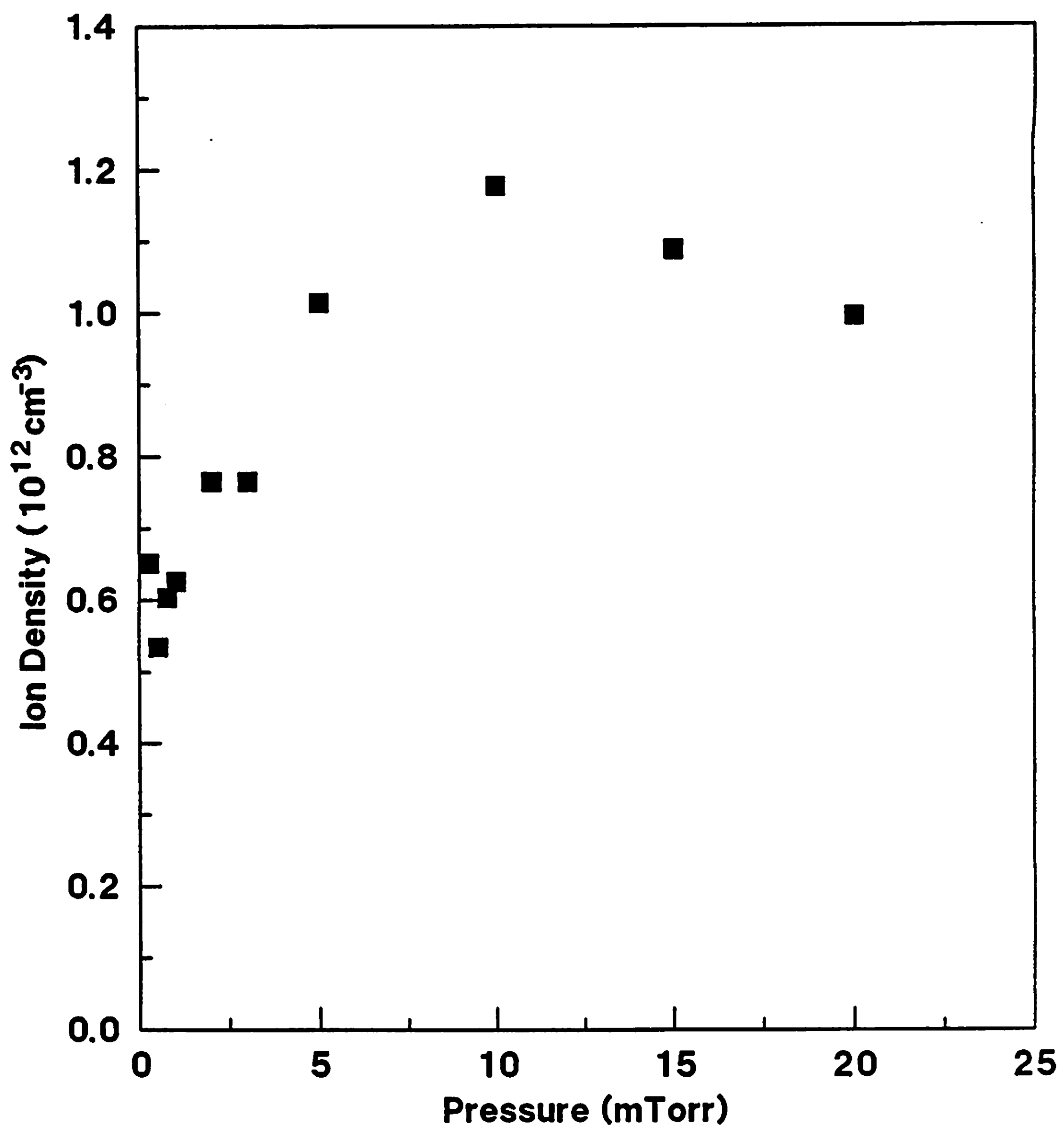

Figure 8(a)

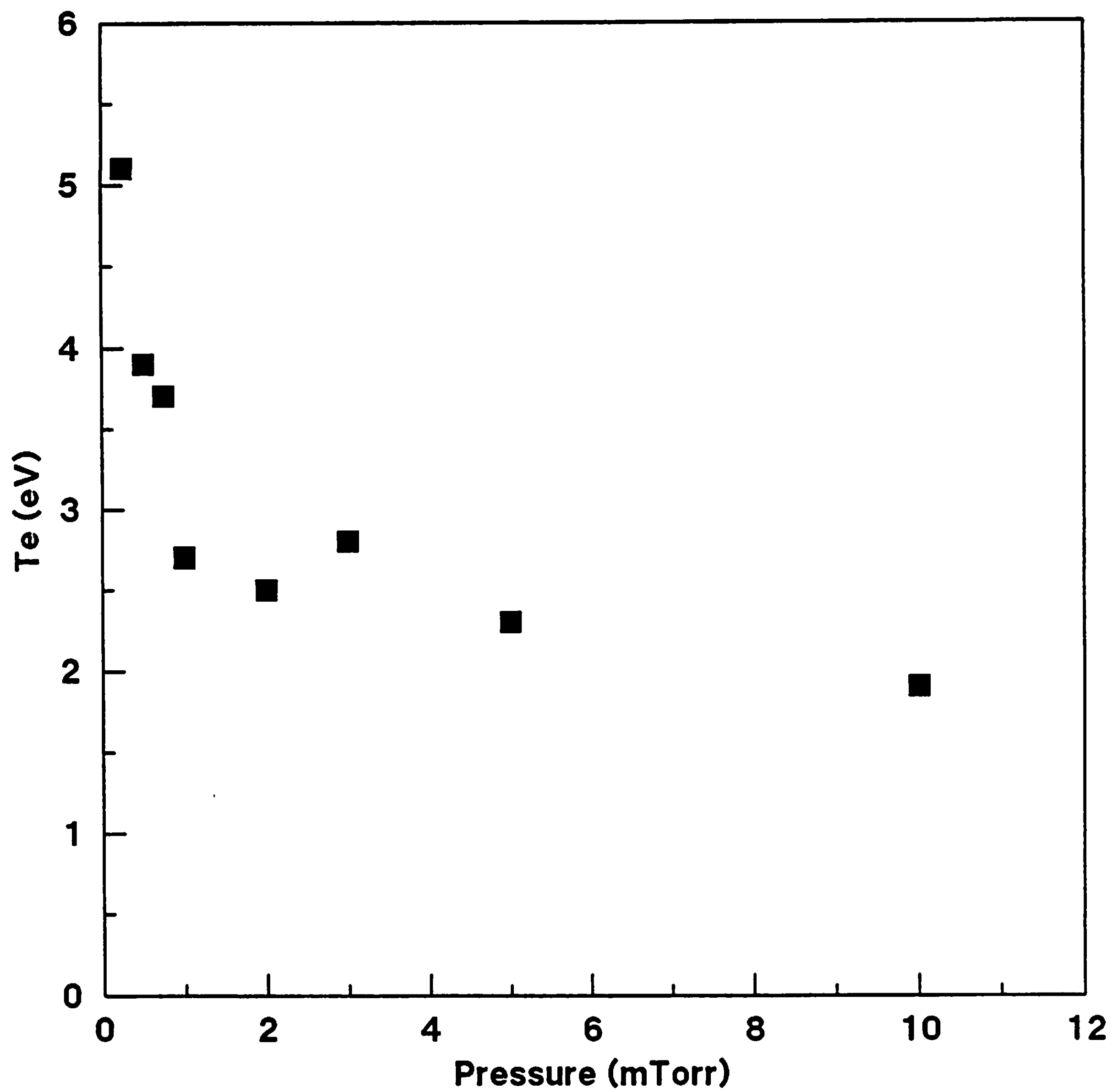

Figure 8(b)

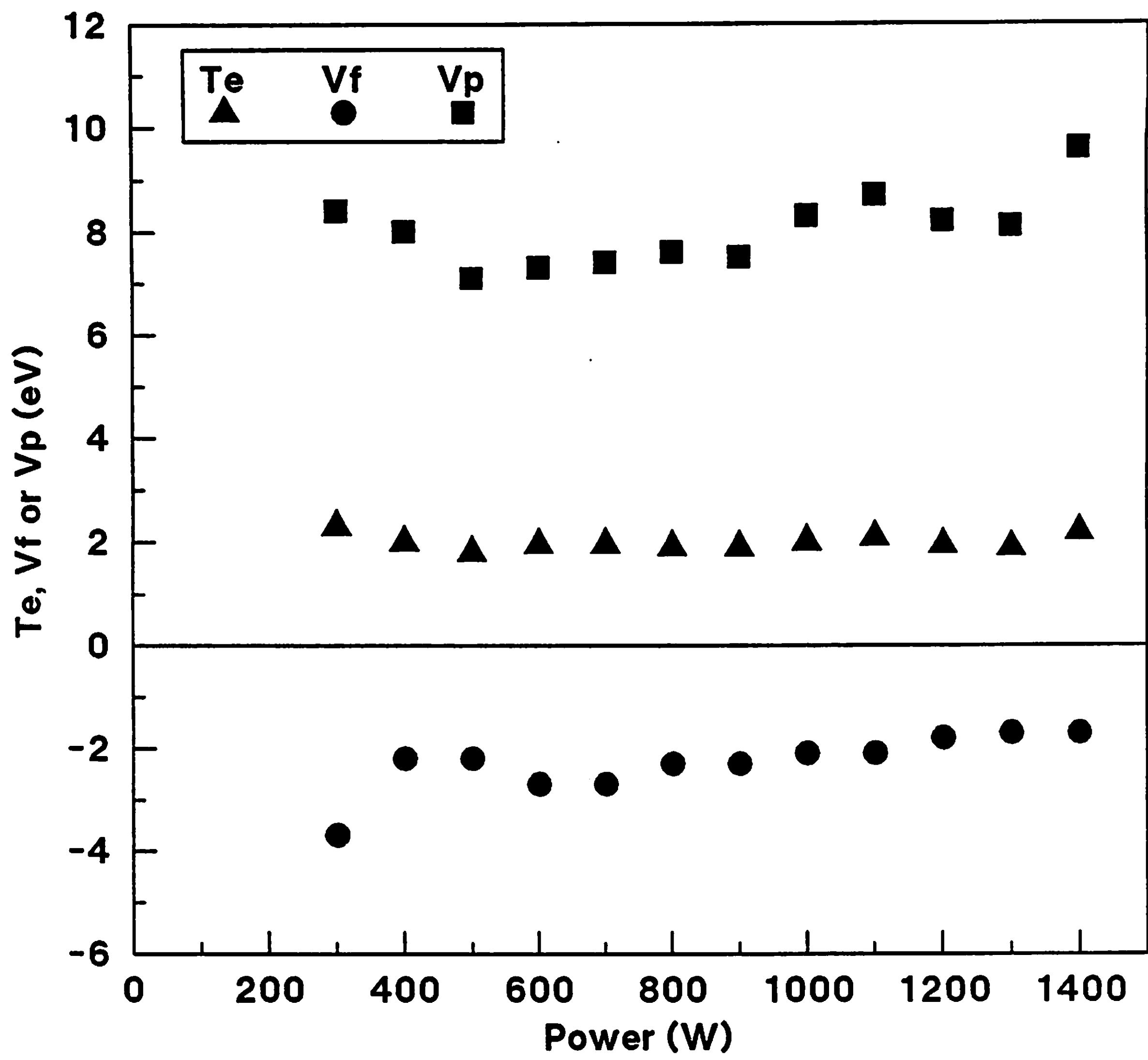

Figure 9

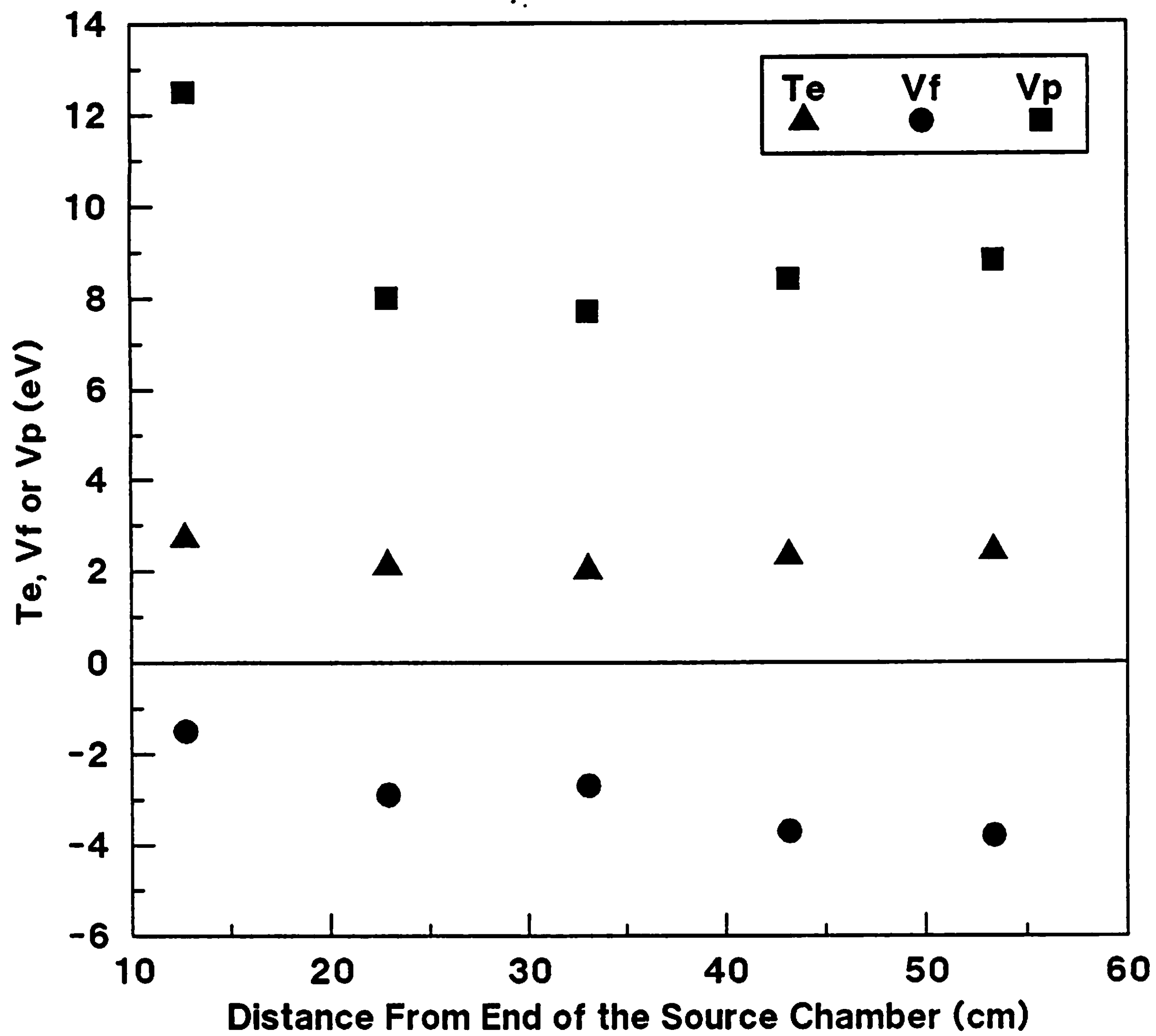

Figure 10

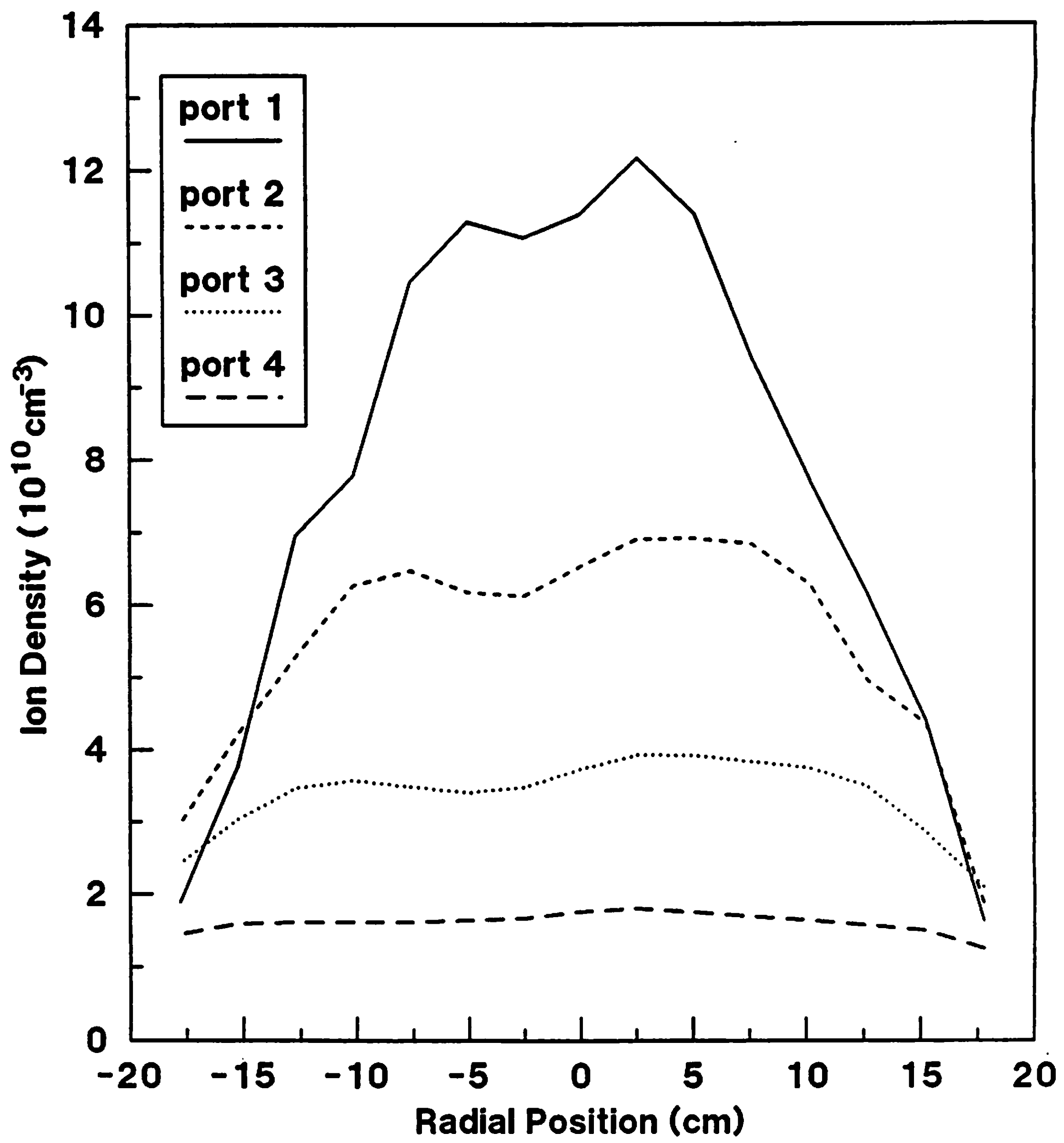

Figure 11

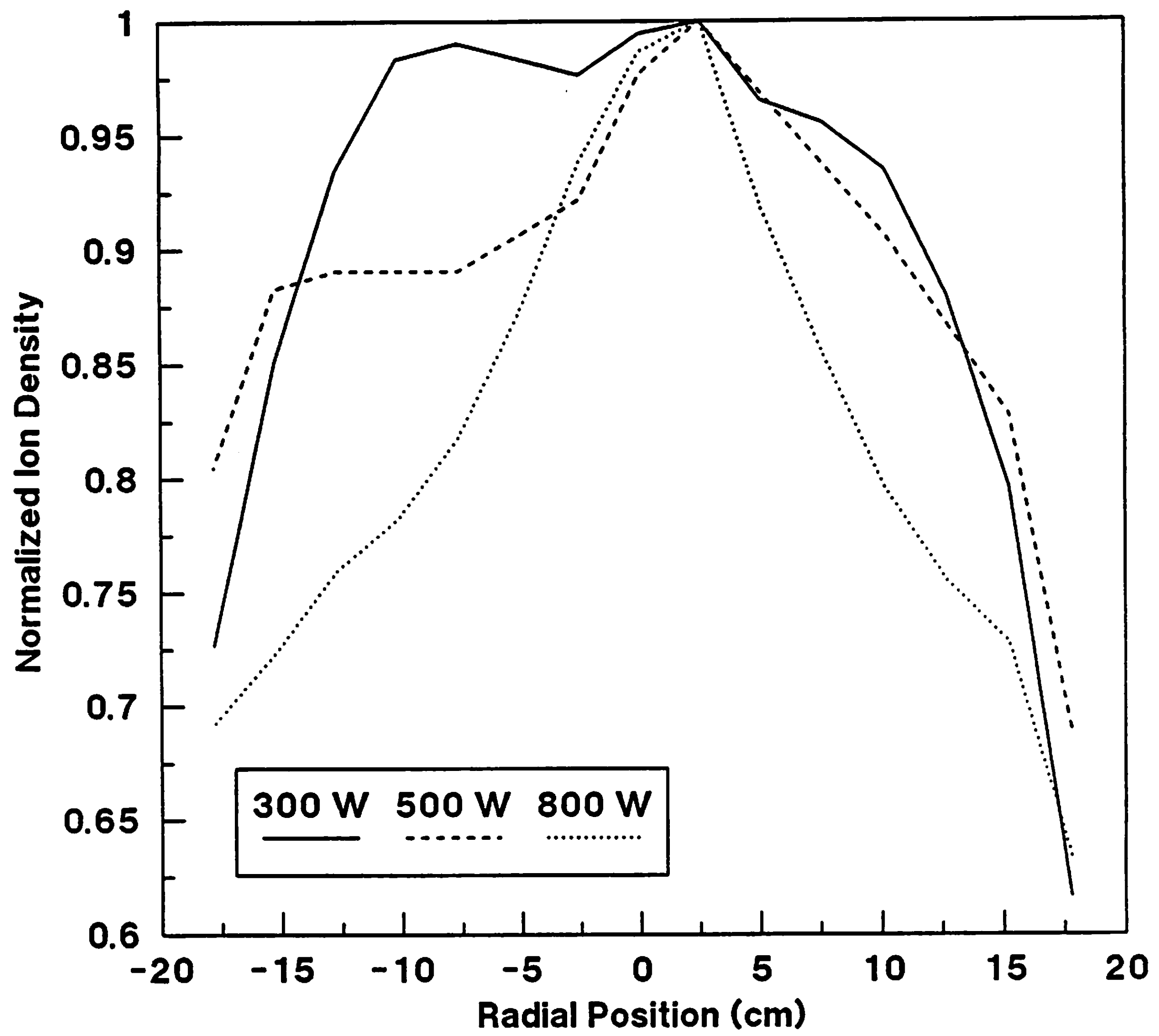

Figure 12

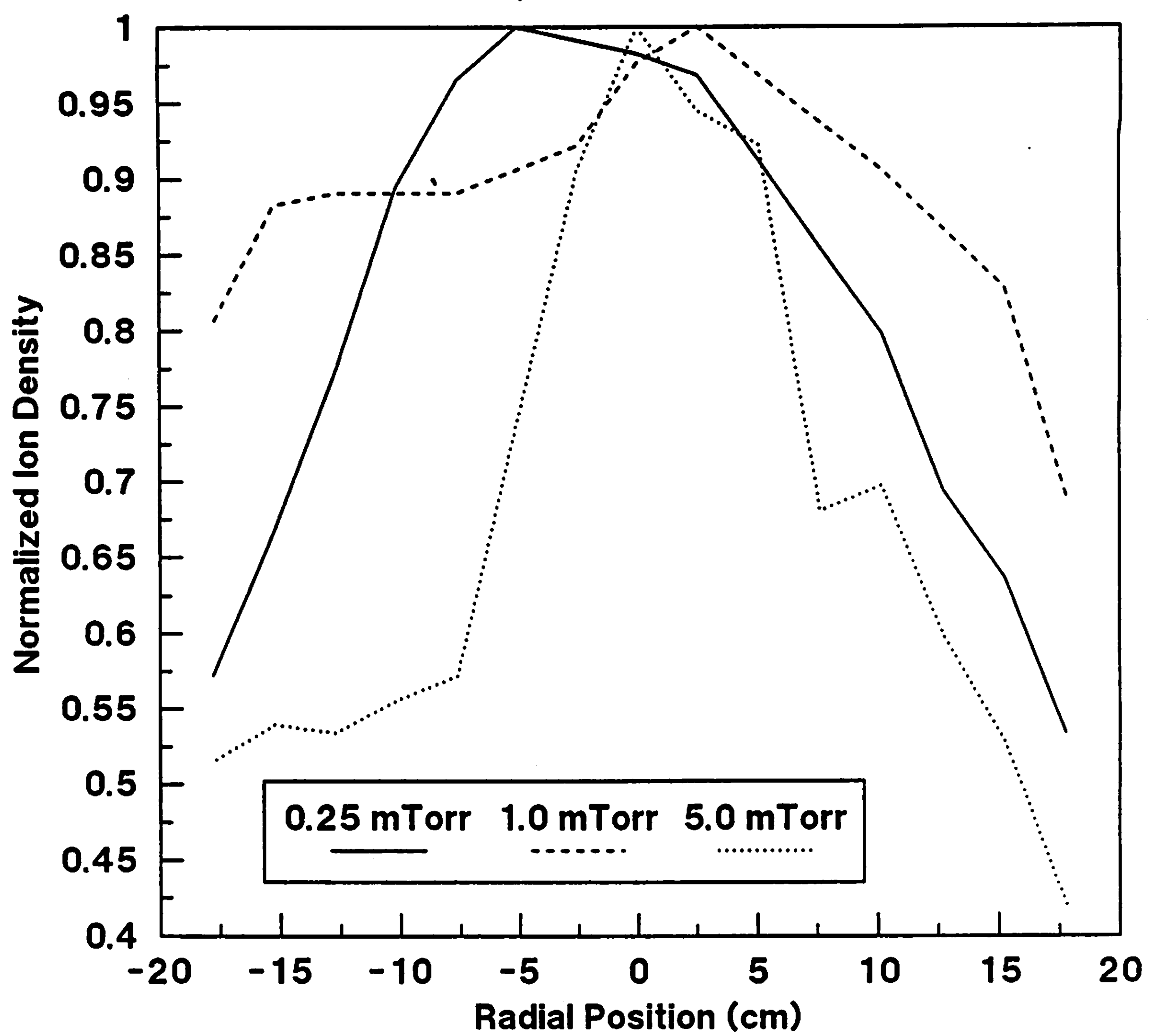

Figure 13

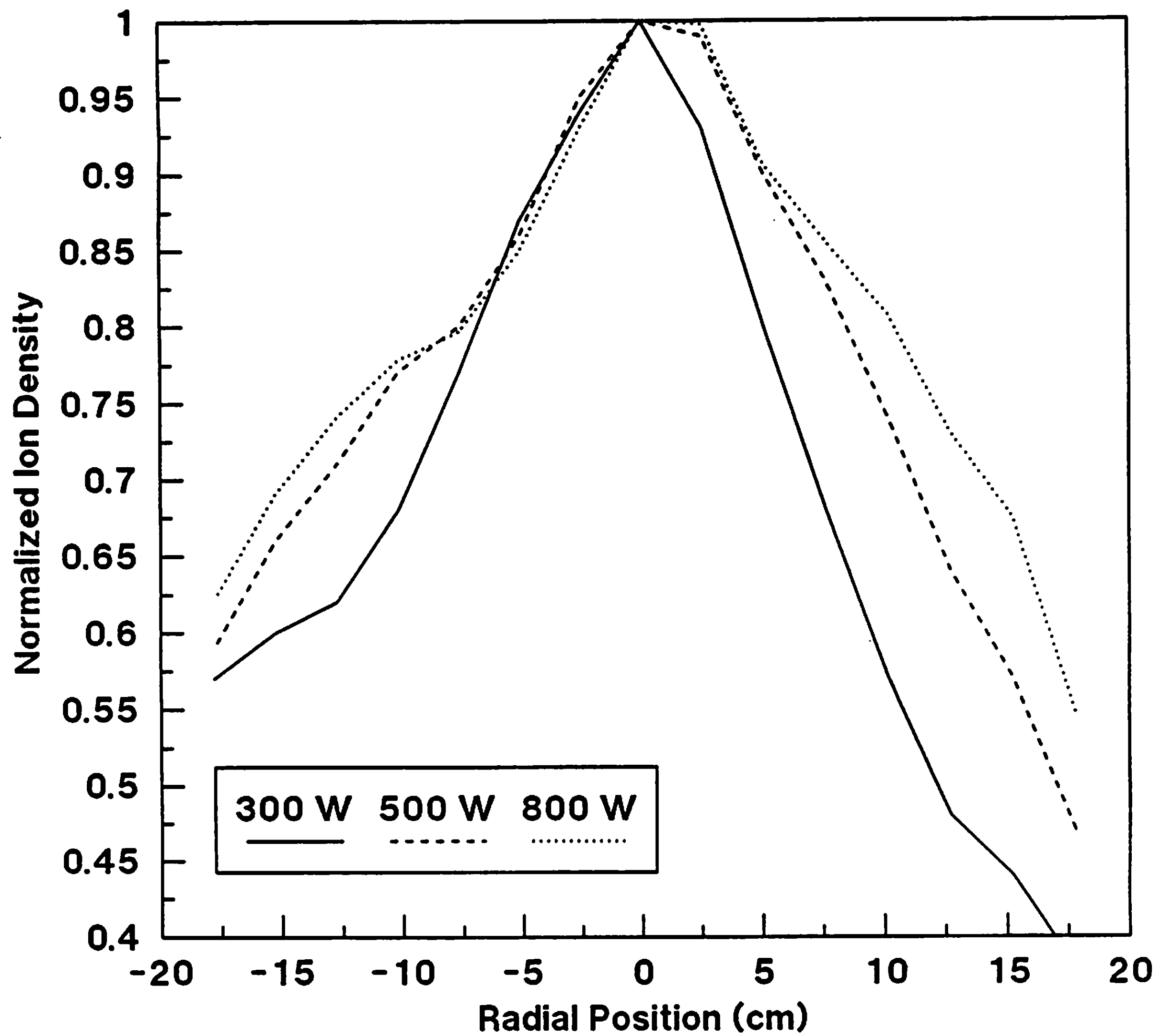

Figure 14

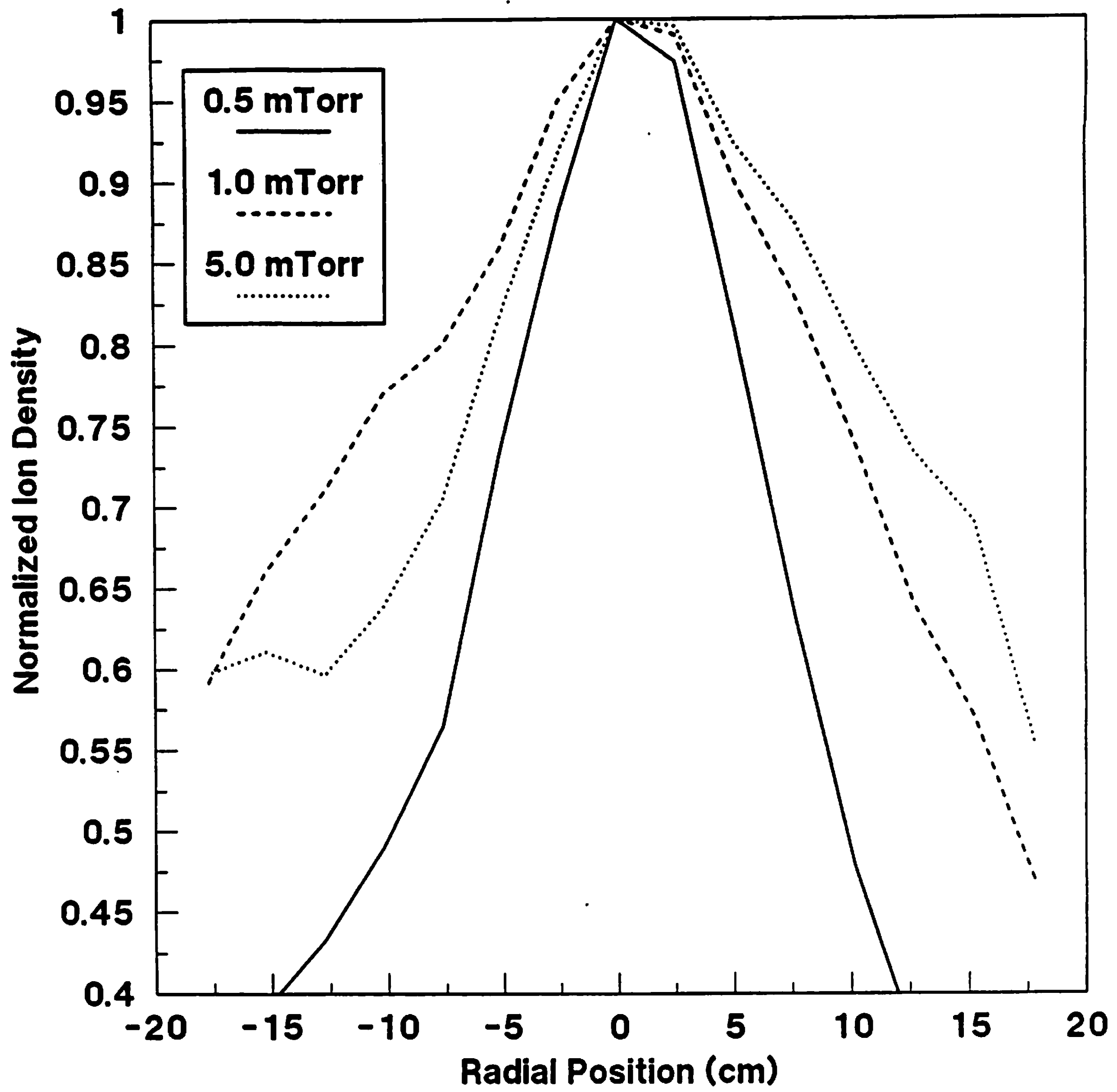

Figure 15

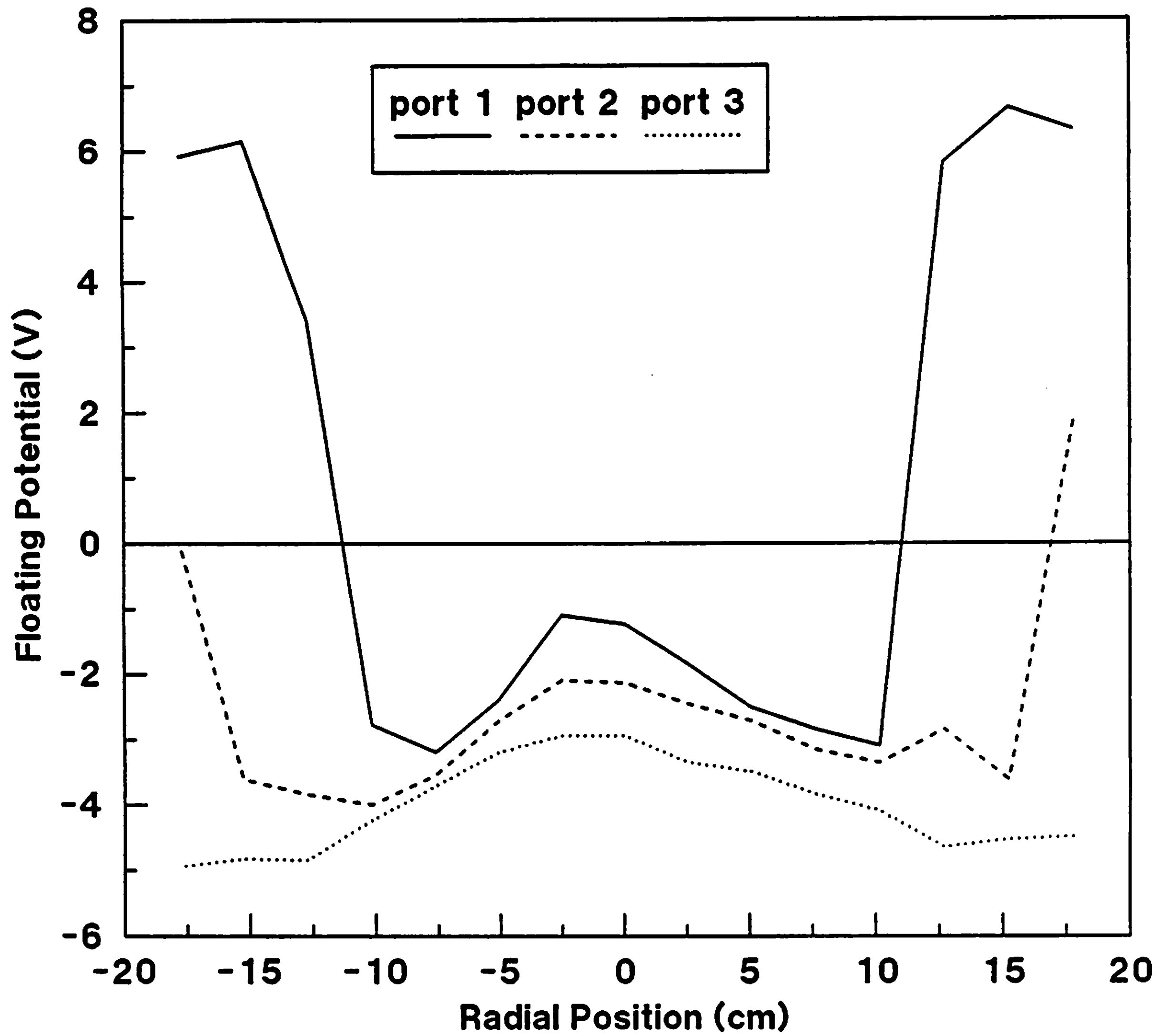

Figure 16